



Evaluation of Mesoporous Silica Nanoparticles as Delivery Vehicles for Novel Hybrid Steroids in Management of Metabolic Syndrome in Mice



CrossMark

Dina S. El-kady^a, Mostafa Mabrouk^b, Soheir E. Kotob^a, Mervat M. Abdelhalim^a, Gamal A. Elmegeed^a, Hanan H. Behierei^b, Hanaa H. Ahmed^{a*}

^a Hormones Department, Medical Research Division, ^b Refractories, Ceramics and Building materials (Biomaterials) Department, National Research Centre, Dokki, Giza, Egypt
(Affiliation ID: 60014618)

Abstract

This approach aimed to address the efficacy of the newly synthesized hybrid steroids modified by sulfur heterogenous rings and loaded on mesoporous silica nanoparticles in manipulating metabolic syndrome induced by high fructose diet. The designed compounds were synthesized by mechanochemical process and then loaded on mesoporous silica nanoparticles as drug delivery vehicles. Thereafter, these compounds were examined for counteracting metabolic syndrome in mice. The synthesized compounds revealed potentiality to prevent body weight gain as indicated by the decreased BMI of the mice fed high fructose diet. The hypolipidemic effect of the designed compounds was evidenced by the reduction of serum cholesterol, triglycerides, LDL-cholesterol and the enhancement of HDL-cholesterol levels. Moreover, the compounds displayed a significant decline in blood glucose and insulin levels. So, they exhibited significant betterment in insulin resistance of the treated mice. Furthermore, the treatment with these compounds improved serum spexin level in metabolic syndrome-challenged mice. Ultimately, the tested compounds demonstrated powerful free radical scavenging activity manifested by lowering MDA, NO and H₂O₂ serum levels. Conclusively, the newly modified hybrid steroid compounds proved good performance against metabolic syndrome in mice most probably due to their content of sulfur atom, in addition to their loading on mesoporous silica nanoparticles.

Keyword: mesoporous silica, nanoparticles drug delivery, hybrid steroids, metabolic syndrome, mice.

1- Introduction

Obesity and its associated metabolic comorbidities represent a growing public health problem [1]. The epidemiological data have demonstrated that metabolic syndrome (MetS), is recognized by central obesity, enhanced fasting blood glucose, dyslipidemia, and elevated blood pressure [2]. Adiposity constitutes the most potent leading power for the development of insulin resistance (IR) and type 2 diabetes. Rising evidence points to "adipose dysregulation", rather than fat mass accrual per se, as a vital pathophysiological cause of the obesity-associated metabolic complications. The dysfunctional fat, in addition to hypertrophic fat cells and inflammatory signals, causes a depressed ability to form new adipocytes from the undifferentiated precursor cells (ie, the preadipocytes). The impairment of adipogenesis leads to a "diabetogenic" milieu either by enhancing the ectopic overflow/deposition of lipids in non-adipose targets (lipotoxicity) or by stimulating a

dysregulated production of various adipose-derived hormones (ie, adipokines and lipokines). This novel and exciting pattern ("expandability hypothesis") further extend current "adipocentric view" comprising a reduced adipogenic capacity as a missing loop between "unhealthy" fat expansion and deterioration of metabolic homeostasis. Interestingly, there are compelling circumstantial data indicating that lipid peroxidation by-products may detrimentally affect adipose homeostasis partially by weakening preadipocyte differentiation. In this scenario, it is tempting to hypothesize that a fine tuning of the adipose redox condition may deliver new mechanistic insights into the link between fat dysregulation and the development of metabolic dysfunctions [3].

Current treatment of MetS and its associated disorders has relied on pharmacological therapies [4]. Meanwhile, in addition to the short-term benefits and their use for symptoms only [5], the pharmaceutical therapies are notified for their restricted effectiveness and serious adverse events

*Corresponding author e-mail: hanaaomr@yahoo.com

Receive Date: 29 January 2021, Revise Date: 10 May 2021, Accept Date: 23 May 2021

DOI: 10.21608/EJCHEM.2021.57952.3295

©2021 National Information and Documentation Center (NIDOC)

in the long-term duration of treatment [6]. Moreover, the long period of treatment or the combination of diverse drugs to treat MetS may enhance the risks of other diseases and even become life-threatening [7]. Understanding the mechanisms involved in the development of metabolic syndrome is of great interest to prevent or reduce its pathological patterns [8].

Steroids administration in cases of MetS tends to lower body fat [9] but unfortunately about 90% of an oral dose of steroids are metabolized before they reach the systemic circulation [10]. Thus, the combination of two distinct and independently acting compounds into one covalently linked hybrid compound could achieve a synergistic effect from both independently acting moieties to the new composite compound. This leads to a pharmacological intensity better than each singular moiety [11].

Researches in nanotechnology expanded over the last decade, introduced several prerequisites for drug delivery systems. Nanoparticles used in nanomedicine as drug carriers should have a high loading capacity and the loaded drug should be preserved until it reaches the site of action. Importantly, such nanoparticles should have a good biocompatibility which does not only depend on the utilized material, but also affected by degradation and excretion. Moreover, these nanoparticles should be taken up typically and efficiently by the cells and passed the mononuclear phagocytic system (MPS). Thus, once, the drug carriers are integrated into the cells, and the drug release is critical [12].

Mesoporous silica nanoparticles are considered as an excellent representative for biodegradable drug carriers. The distinct structure of mesoporous silica allows high loading capacity and the plethora of surface modifications improves the efficacy of the drug and reduces its side effects [13]. An *in vivo* research proposed that the prepared insulin loaded mesoporous silica nanoparticles (MSNs) are capable to reduce the blood glucose concentration for up to 10 h in streptozotocin-induced diabetic rat [14]. Interestingly, one study demonstrated a smart system and functionalized MSNs for glucose responsive delivery of and their real-time monitoring for accurate quantification [15].

The current study was designed to synthesize newly hybrid steroid compounds through the combination of steroid moiety with structural elements possessing appropriate restrained activity on fat deposition. Moreover, the study was extended to

load the synthesized compounds on mesoporous silica nanoparticles as drug delivery vehicles and to investigate the efficacy of these formulations in interfering with metabolic syndrome in the experimental model.

2- Experimental

2.1 Materials

Starting steroids molecules were purchased from Sigma Company, USA. All solvents were anhydrous by distillation prior to using. All melting points were measured using an electrothermal apparatus. The IR spectra were recorded in (KBr discs) using Shimadzu FT-IR 8201 PC spectrometer and expressed in cm^{-1} . The ^1H NMR and ^{13}C NMR spectra were registered by using a Jeol instrument (Japan), at 270 and 125 MHz respectively, in DMSO-d_6 as solvent and the chemical shifts were recorded in ppm relative to TMS. The spin multiplicities were abbreviated by the letters: s-singlet, d-doublet, t-triplet, q-quartet and m –multiplet (more than quartet). Mass spectra were recorded on a GCMS-QP 1000 ex spectra mass spectrometer operating at 70 eV. Elemental analyses were carried out by the Microanalytical Data Unit at the National Research Centre, Giza, Egypt and the Microanalytical Data Unit at Cairo University, Giza, Egypt. The reactions were monitored by thin layer chromatography (TLC) which was carried out using Merck 60 F254 aluminum sheets and visualized by UV light (254 nm). The mixtures were separated by preparative TLC and gravity chromatography. All steroid derivatives showed the characteristic spectral data of cyclopentanoperhydrophenanthrene nuclei of androstane series that were similar to those reported in the literature [16].

2.2 Methods

2.2.1 Synthesis of compound (7) to (11):-

Mechanochemical processes are both solvent-free and less energy consuming methods than the standard solution reactions methods and they are rapidly becoming popular as green processes alternative to conventional solution-based processes [17]. The perfectly 'green' reaction proceeds at room temperature, requires no organic solvent, highly selective, exhibits high atom efficiency, and yet produces no waste products [18].

General procedure

A mixture of the appropriate carbonyl compound 1-5 (1 mmol) and thioglycolic acid (1.5 mmol, 0.13 gm) (except in case of progesterone we add excess 2 mmol) was thoroughly grounded in an agate mortar. The grinding was continued until completion of the reaction (4 min), as monitored by TLC. On completion of the reaction, the mixture became a solid mass which was treated with water. The resultant product was filtered and washed with water, recrystallized from appropriate solvent and dried under vacuum to yield the pure products.

(8-R,9S,10R,13S,14S,17S)-10,13-dimethyl-5'-oxo-1,2,6,7,8,9,10,11,12,13,14,15,16,17-tetradecahydrospiro[cyclopenta[a]phenanthrene-3,2'-[1,3]oxathiolan]-17-yl acetate(7)

White powder, from absolute ethanol. Yield = (3.67 gm) 90 %, mp 146-148 ° C. IR (kBr, cm⁻¹): ν 2945-2847 (CH-aliphatic), 1728 (2 C=O), 1620 (C=C). ¹H NMR (DMSO-d₆, ppm): δ = 0.78(s, 3H, CH₃-19), 1.63-2.51 (m, steroid moiety), 1.91 (s, 3H, CH₃-18), 2.49 (s, 3H, CH₃-Ac), 3.31(s, 2H, CH₂-oxathiolane), 5.42(m, 1H, C4-H). ¹³C NMR (DMSO-d₆, ppm): δ = 27.5 (C-1), 36.6(C-2), 130.1(C-4), 140.8 (C-5), 31.4 (C-6), 31.1 (C-7), 34.6 (C-8), 50.0 (C-9), 39.3 (C-10), 20.6 (C-11), 36.65 (C-12), 42.5(C-13), 50.7 (C-14), 23.4 (C-15), 27.5(C-16), 82.2 (C-17), 12.3(C-18), 19.01 (C-19), 170.8 (C=O), 21.3 (C-CH₃), 34.3(C-O). MS (EI) m/z =404 M⁺, 68%, 389 (3), 313(16), 253 (33), CalcM.wt for C₂₃H₃₂O₄S (404.20).

(8R,9S,10S,13R,14S,17R)-10,13-dimethyl-17-((R)-6-methylheptan-2-yl)hexadecahydrospiro[cyclopenta[a]phenanthrene-3,2'-[1,3]oxathiolan]-5'-one(8)

White powder, from absolute ethanol. Yield = (3.40 gm) 74%, mp 117-118 ° C. IR (kBr, cm⁻¹): ν 2929-2859 (CH-aliphatic), 1716 (C=O). ¹H NMR (DMSO-d₆, ppm): δ = 0.83 (s, 3H, CH₃-19), 1.04-2.49 (m, steroid moiety), 0.85 (s, 3H, CH₃-18), 0.96 (d, 2H₃, 2CH₃), 1.04(m,2H,CH₂), 1.40(q, 2H, 2CH), 1.65(q, 2H₂, 2CH₂), 2.68 (d, 1H, C4-H), 3.30(s, 2H, CH₂-oxathiolane). ¹³C NMR (DMSO-d₆, ppm): δ = 29.00 (C-1), 31.80 (C-2), 93.50 (C-3), 37.40 (C-4), 38.21 (C-5), 28.70 (C-6), 32.00(C-7), 35.30 (C-8), 51.80 (C-9), 34.20 (C-10), 20.70 (C-11), 40.20 (C-12), 42.80 (C-13), 56.60 (C-14), 24.20 (C-15), 28.20 (C-16), 55.80 (C-17), 13.80 (C-18), 13.00 (C-19), 172.60 (C=O), 28.10, 35.10 (CH-aliphatic), 24.70, 38.20, 39.99(3CH₂-aliphatic), 19.3, 23.10, 23.30(3CH₃-aliphatic) 33.90(C-oxathiolane). MS (EI) m/z = 460 M⁺, 79%, 445(41), 403(25), 358(55), 316(17). CalcM.wt for C₂₉H₄₈O₂S (460.338).

(3S,8R,9S,10S,13S,14S)-10,13-dimethyl-5'-oxohexadecahydrospiro[cyclopenta[a]phenanthrene-17,2'-[1,3]oxathiolan]-3-yl acetate(9)

White powder, from absolute ethanol. Yield = (3.04 gm) 75 %, mp 65 ° C. IR (kBr, cm⁻¹): ν 2929-2856(CH-aliphatic), 1733 (2C=O). ¹H NMR (DMSO-d₆, ppm): δ = 0.77 (s, 3H, CH₃-19), 1.22-1.96 (m, steroid moiety), 0.80 (s, 3H, CH₃-18), 0.96 (s, 2H, CH₂- oxathiolane), 4.50 (m, 1H, C₃-H), 2.50(s, 3H, CH₃-Ac). ¹³C NMR (DMSO-d₆, ppm): δ = 35.77 (C-1), 27.57 (C-2), 73.28 (C-3), 31.81 (C-4), 40.19 (C-5), 28.63 (C-6), 31.77(C-7), 34.91 (C-8), 54.04 (C-9), 35.00 (C-10), 20.55 (C-11), 30.79 (C-12), 51.13 (C-13), 51.05 (C-14), 13.91 (C-15), 37.07 (C-16), 12.36 (C-18), 12.55 (C-19), 170.28, 170.86 (2C=O), 21.55 (C-Ac), 34.11(C-oxathiolane). MS (EI) m/z = 406 M⁺, 15%, 391(11), 316(11), 276(18), 242(16). CalcM.wt for C₂₃H₃₄O₄S (406.218).

(8R,9S,13S,14S)-13-methyl-5'-oxo-6,7,8,9,11,12,13,14,15,16-decahydrospiro[cyclopenta[a]phenanthrene-17,2'-[1,3]oxathiolan]-3-yl acetate(10)

White powder, from absolute ethanol. Yield = (2.43 gm) 63 %, mp 125 ° C. IR (kBr, cm⁻¹): ν 2929-2861 (CH-aliphatic), 1718 (2C=O), 1619 (C=C). ¹H NMR (DMSO-d₆, ppm): δ = 0.83 (s, 3H, CH₃-18), 1.33-2.75 (m, steroid moiety), 2.31(s, 3H, CH₃-Ac), 3.34 (s, 2H, CH₂- oxathiolane), 6.46-7.31 (m, aromatic moiety). ¹³C NMR (DMSO-d₆, ppm): δ = 126.74 (C-1), 119.37 (C-2), 148.78 (C-3), 122.00 (C-4), 137.58 (C-5), 29.52 (C-6), 26.60(C-7), 37.95 (C-8), 44.01 (C-9), 138.20 (C-10), 26.26 (C-11), 29.32 (C-12), 47.80 (C-13), 47.75 (C-14), 21.03 (C-15), 31.84 (C-16), 113.26 (C-17), 13.95 (C-18), 155.49 (2C=O), 21.60 (C-Ac), 35.84(C-S). MS (EI) m/z = 386 M⁺, 37 %, 371(20), 296(19), 252(20), 187(28). CalcM.wt for C₂₂H₂₆O₄S (386.155).

(8S,9S,10R,13S,14S,17S)-10,13-dimethyl-17-((R)-2-methyl-5-oxo-1,3-oxathiolan-2-yl)-1,2,6,7,8,9,10,11,12,13,14,15,16,17-tetradecahydrospiro[cyclopenta[a]phenanthrene-3,2'-[1,3]oxathiolan]-5'-one (11)

Yellow powder, from absolute ethanol. Yield = (4 gm) 86 %, mp 95-97 ° C. IR (kBr, cm⁻¹): ν 2925 (CH-aliphatic), 1698 (2 C=O), 1635 (C=C). ¹H NMR (DMSO-d₆, ppm): δ = 0.92 (s, 3H, CH₃-18), 1.23-2.07 (m, steroid moiety), 1.28 (s, 3H, CH₃-19), 1.48(q, 2H, CH₂ -16), 1.62(s, 3H, CH₃), 2.35(t,1H, CH-17), 3.72 (s, 2H₂, 2 CH₂- oxathiolane), 5.40(s, 1H, CH-4). ¹³C NMR (DMSO-d₆, ppm): δ = 28.00 (C-1), 36.00 (C-2), 95.00 (C-3), 32.20 (C-6), 31.00 (C-7), 35.50 (C-8), 56.00 (C-9), 37.00 (C-10), 21.90 (C-11), 39.40 (C-12), 36.20 (C-13), 55.80 (C-14), 24.80 (C-15), 20.20 (C-16), 55.60 (C-17), 14.70 (C-18), 19.90(C-19), 172.00 (C=O), 33.70 (C-S), 140.80

(C=C), 27.40 (C-methyl). MS (EI) $m/z = 463 M^{+1}$, 19 %, 372(12), 345(56), 330(33), 319(34). CalcM.wt for $C_{25}H_{34}O_4S_2$ (462.190).

2.2.2 Preparation of mesoporous silica nanoparticles

Mesoporous silica nanoparticles were prepared by using micro-emulsion technique. In brief, two solutions were prepared for this purpose, solution A that was prepared by dissolving of 4 g of poly vinyl alcohol (PVA) in co-solvent of 250 mL distilled water and 150 mL ethanol and the stirring was continued at 70°C. After complete dissolving of PVA, 0.8 g of cetyltrimethyl ammonium bromide (CTAB) was added and dissolved within the PVA solution. Meanwhile, solution B was also prepared by mixing of 25 mL tetraethyl-ortho-silicate (TEOS) with 20 mL cyclohexane and was stirred for 30 min. Then solution B was dropped gradually on a solution A under vigorous stirring for 2 h till the micro-emulsion obtained. The obtained mixture was further dried at 70 °C for overnight. Afterwards, drying process was applied following the next regime. In the beginning, the temperature was raised to 130 °C within 30 min and kept at this temperature for 2 h. Thereafter, it was raised to 350 °C within 2 h and kept at this temperature for 4 h. Finally, it was raised to 600 °C within 2 h and kept at this temperature for 2 h. The collected sample was preserved in desiccator for further investigations.

2.2.3 Drug loading and release

Mesoporous silica nanoparticles (100 mg) were suspended in 100 ml of methanol that was allowed to be stirred under the normal conditions. After 30 min known quantities of **7**, **9** and **11** drugs were dissolved separately in the above mixture and continued stirring for another 30 min. Then, the achieved emulsions were transferred to a shaker incubator with a shaking rate of 200 rpm for 2 h in order to ensure the encapsulation of dissolved drug within the mesoporous silica nanoparticles. Finally, the methanol was completely evaporated and drug-loaded mesoporous silica nanoparticles were collected. The drug loading capacity was determined using a UV spectrophotometer at the wavelengths 243, 240 and 250nm using equation 1. Furthermore, the drug release profile for each drug was evaluated after immersion of the drug-loaded mesoporous silica nanoparticles in 15 ml of phosphate buffer saline (PBS) in measured polypropylene tubes at pH of 7.4 and 37°C for up to 28 days. After each immersion period 3 ml of PBS medium was

collected from the tubes to be analyzed by a UV spectrophotometer at the abovementioned wavelengths and further replaced with fresh PBS in order to keep the sink conditions.

2.2.4 Characterization of the drug-loaded mesoporous silica nanoparticles

In the current study, several techniques have been applied to characterize the under investigated mesoporous silica nanoparticles before and after drug loading. The physicochemical properties were determined by using X-rays diffractometer (XRD). XRD patterns of the powder were collected by using XRD (D8 ADVANCED Cu target; Bruker, USA) diffractometer. To produce monochromatic X-rays, a Cu $K\alpha$ source was used with an emission current of 200mA and a voltage of 40 kV with a wavelength of 0.1542 nm. The measurements were conducted in the range of 2°–70° at a scan speed of 4°/min. To investigate the functional groups of the prepared samples, Fourier transmittance infrared spectroscopy (FTIR) was implemented. KBr disks of 0.5-cm diameter were prepared after mixing with the tested samples (mixing ratio 1: 100 sample: KBr) in the mortar and grinded into a fine powder. Perkin Elmer Spectrum 2000 FTIR spectrometer Demonstrate 1600, Perkin- Elmer (USA), was utilized to record FTIR spectra at a resolution of 4 cm^{-1} . Particle size distribution and zeta potential Dynamic particle size and charge of the prepared nanoparticles were obtained using Dynamic light scattering (DLS) instrument (Zetasizer Nano ZS, Malvern Instruments, UK) equipped with a 633 nm laser. The reference standard (DTS1230, zeta-potential standard from Malvern) was used to qualify the performance of the instrument. Samples (50 mg) were suspended in 10 ml of deionised water; and were filtered using a 0.22 μm filter before analysis. Sample preparation involved filling of a disposable capillary cell (DTS1060, Malvern). The thermal behavior of the prepared samples was investigated by DSC/TGA using a computerized SETARAM Labsys TG-DSC thermal analysis system. Samples (100±1 mg) were placed in the 30-ml platinum crucible with a heating range of 25–1000°C with a heating rate of 10°C/min.

Transmission electron microscopy TEM was used to analyze the size and morphology of the prepared samples. The particle size and appearance of the prepared samples were determined using TEM (JEM-2100; Jeol) at an accelerating voltage of 200 kV.

2.2.5 Ethical statement

This study was conducted in compliance with the standards and the general ethical principles of animal experiments and in accordance with the guidelines of the Ethical Committee for Medical Research of the National Research Centre, Egypt; (Registration Number 18/190).

2.2.6 Animals and housing conditions

Animals were kept in conditions that were accredited in accordance with the standard rules of experimental biological clinics. A total of 90 adult female albino Swiss mice, weighing 25 ± 5 g at 10-week-old, were enrolled in this experimental setting. The animals were obtained from the Animal House facility of the National Research Centre, Giza, Egypt. The animals were housed 5mice/cage in polypropylene cages in an environmentally controlled clean air room with a temperature of $24 \pm 1^\circ\text{C}$, a 12 hrs light/12 hrs dark cycle, a relative humidity of $60 \pm 5\%$ and free access to tap water and standard rodent chow. The mice were allowed to adapt to these conditions for 2 weeks before the commencement of the experiment.

2.2.7 Animal grouping

After the acclimation period, a group of ten mice was fed a standard rodent chow with 26.5% protein, 3.8% fat, 40% carbohydrate, and 4.5% crude fiber according to **Buettner et al.** [19] during 16 W of the experimental period and served as lean control group (control group). All other mice (80 mice) were fed 65% high fructose diet (HFD) for 8 weeks. The percent of fructose and the duration of high fructose feeding were selected on the base of the previous study for induction of MetS in animals described by **Bagul et al.** [20]. The HFD was composed of the following ingredients: casein 200g, DL-methionine 3g, fructose 650g, cellulose 50g, corn oil 50g, salt mix 35g, vitamin mix 10g and choline bitartamicee 2g; a total of 1000g. Mice with MetS were divided into 8 groups as follows: untreated MetS bearing mice (MetS group); MetS bearing mice treated orally with SMC (1 mg/mL PBS) in a volume of 200 μL /mouse/day according to **Jiang et al.** [21] for 8 Weeks (MetS+SMc); MetS bearing mice treated orally with S7 for 8 Weeks (MetS+S7); MetS bearing mice treated orally with S 9 for 8 Weeks (MetS+S 9); MetS bearing mice treated orally with S11 for 8 Weeks (MetS+S11); MetS bearing mice orally treated with 7 for 8 Weeks (MetS+7); MetS bearing mice treated orally with 9 for 8 Weeks (MetS+9) and MetS bearing mice treated orally with 11 for 8 Weeks (MetS+11). Of note, the all synthesized compounds were administered orally in a dose of 1 mg/mL PBS in a volume of 200 μL /mouse/day.

2.2.8 Anthropometric measurements

At the end of the experimental period (16 W), the abdominal circumference (AC) (immediately anterior to the forefoot), thoracic circumference (TC) (immediately behind the foreleg), and body length (nose-to-anus length) were measured in anesthetized mice. Body weight and body length were measured to be used for determination of body mass index (BMI) [22].

$$\text{BMI (g/cm}^2\text{)} = (\text{Body weight (g)}/\text{Length}^2 \text{(cm}^2\text{)})$$

2.2.9 Samples collection

After obtaining the anthropometric parameters, the mice were fasted overnight (12-14 hrs), and the blood samples were drained, under diethyl ether anesthesia, from the retroorbital venous plexus in clean dry centrifuge tubes and allowed to coagulate for 45 minutes at room temperature to obtain sera. Serum samples were separated by centrifugation at $1800 \times g$ for 15 minutes at 4°C using cooling centrifuge. Aliquots of serum samples were frozen and stored at -20°C pending further biochemical analyses. After collection of blood samples, the mice were scarified by cervical dislocation.

2.2.10 Biochemical evaluation

Serum total cholesterol, triglycerides (TG), high-density lipoprotein (HDL), low-density lipoprotein (LDL) and glucose levels were estimated by colorimetric method using kits purchased from Reactivos GPL (Barcelona, Spain) following the methods of [23-26] respectively. Serum insulin level was quantified using enzyme-linked immunosorbent assay (ELIZA) kit purchased from Epitope Diagnostics, Inc. Co. (USA) following the method of [27]. The homeostasis model assessment of basal insulin resistance (HOMA-IR) was used to calculate the index from the product of the fasting concentration of serum glucose (mmol/L) and serum insulin ($\mu\text{U/L}$) divided by 22.5 according to the method of [28]. Serum H_2O_2 , malondialdehyde (MDA) and nitric oxide (NO) levels were measured by colorimetric method using kits purchased from Biodiagnostic Co., Egypt, according to [29-31] respectively. Quantitative assessment of serum spexin level was carried out using ELIZA kit purchased from NOVA (China) according to manufacturer's instruction.

2.2.11 Statistical processing

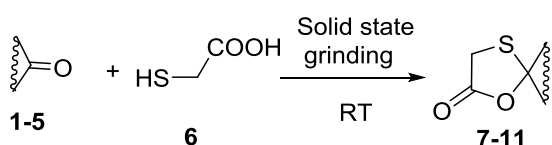
The experimental results were represented as arithmetic means with their standard errors (SE) (mean \pm SE). Data were analyzed by one-way analysis of variance using the Statistical Package for the Social Sciences program, version 20 followed by

least significant difference to compare significance between groups [32]. The P value $P < 0.05$ was ascribed significant. The p-value is the probability of obtaining results at least as extreme as the observed results of a statistical hypothesis test.

3 Results and Discussion

3.1 Chemistry

Reaction of steroids (testosterone, cholestanone, epiandrosterone, esteron and progesterone) with thioglycolic acid at room temperature using grinding mortar for 4 min afforded 1,3-oxathiolane derivatives **7-11** in good yield (scheme 1). ^1H NMR spectra of the new products exhibit, in addition to the expected signals of steroid moiety, CH_2 signal of oxathiolane ring. Besides that, The IR spectra of 1,3-oxathiolane derivatives (**7-11**) revealed strong absorption bands at 1728, 1716, 1733, 1718, and 1798 cm^{-1} respectively attributed to $\text{C}=\text{O}$. The ^{13}C NMR, and equilibrator inlet mass spectrometry (EIMS) analyses agreed completely with the expected structure (cf. "Materials and Methods").



Scheme 1

Table (1): Chemical structure of the newly synthesized compounds

| o. | Structure | o. | Structure |
|----|-----------|----|-----------|
| 1 | | 7 | |
| 2 | | 8 | |
| 3 | | 9 | |
| 4 | | 10 | |
| 5 | | 11 | |

3.2 Physicochemical properties of drug-loaded silica

The physicochemical properties of the drug-loaded silica with reference to the plain silica were investigated using X-ray diffractometer (XRD) and Fourier-transform infrared spectroscopy (FTIR). Figure (1) represents the XRD analyses obtained from all samples. The XRD graphs of samples **S7**, **S9** and **S11** showed amorphous patterns similar to XRD pattern of the pure silica with reflection at $2\theta = 15-30^\circ$ [15]. These findings indicate the complete inclusion of the drugs within the silica pores. However, some minor peaks were detected in the XRD patterns of Silica- **9** and Silica- **11** thus, indicates the presence of drug residues on the silica surface.

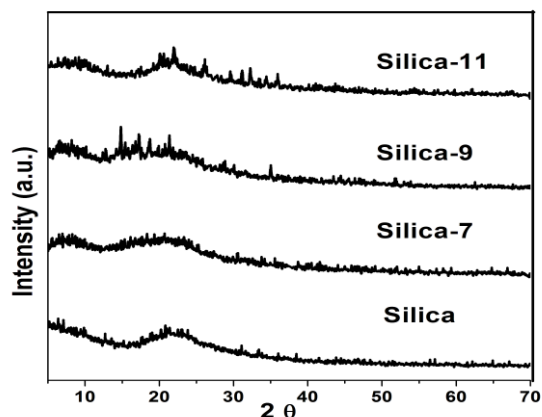


Fig (1): The XRD patterns of drug-loaded silica nanoparticles compared to the drug free silica nanoparticles.

The functional groups of the drug-loaded silica compared to the drug-free silica nanoparticles were illustrated in Figure (2). The pure silica nanoparticles (drug free silica nanoparticles) showed the presence of functional groups at 475, 806, 1099, 1635 and 3423 cm^{-1} . The band observed at 3423 cm^{-1} attributed to surface hydroxyl groups (stretching mode), and the absorption band at 1635 cm^{-1} indicated the presence of adsorbed water (the $\text{Si}-\text{H}_2\text{O}$ flexion). Also, bands characteristic of pure silica, such as the stretching vibration at 1099 cm^{-1} and the bands at 806 cm^{-1} , has been noticed in the spectrum [33]. On the other side, the absence of bands at 550, 1500, 2900 and 3000 cm^{-1} responsible for the CH_2 and CH_3 groups in CTAB molecule and PVA (the pore formers) was confirmed as described by [34]. Interestingly, the drug-loaded silica FTIR spectra for samples Silica-7, Silica-9 and Silica-11 showed the presence of new bands at 1627 cm^{-1} and 1750 cm^{-1} which corresponded to the $\text{C}=\text{C}$ double bonds and $\text{C}=\text{O}$ double bonds, respectively. In

addition, band located at 1280cm^{-1} assigned to aromatic C-O as well as the presence of the band at 2929cm^{-1} ascribed to the C-H functional group [35-37].

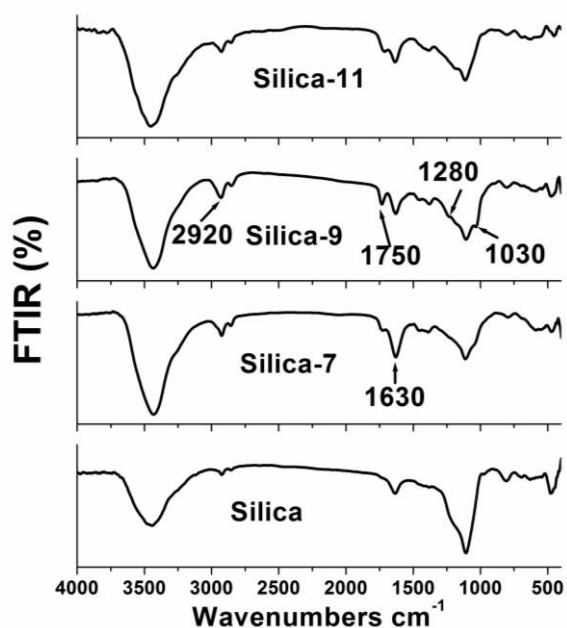


Fig. (2). FTIR spectra of the silica nanoparticles before and after drug loading

3.3 Thermal behavior of drug- loaded silica

In order to evaluate the drug loading on the thermal behaviour of silica nanoparticles, DTA/ TGA thermographs were recorded before and after drug loading. The peak detected at 96°C , corresponding to adsorbed water from the atmosphere, was observed in all the samples, but it was more pronounced for the drug-loaded silica nanoparticles. The thermograms of drug-loaded silica nanoparticles showed characteristic single melting endothermic peak at 230°C (Figure 3) which was not detected in the drug-free silica nanoparticles. Furthermore, the Tg temperature for the drug-free silica nanoparticles was detected at broad exothermic peak in the range of $300\text{--}550^\circ\text{C}$. This peak was shifted and broadened to the range of $525\text{--}660^\circ\text{C}$ in the case of drug- loaded silica nanoparticles. Furthermore, the TGA results exhibited weight loss percent (%) consistence with the DTA results. The total weight loss of the drug-loaded silica nanoparticles at the end of the run was $55 \pm 1.12\%$ compared to the drug-free silica nanoparticles (21 ± 1.42), indicating the presence of the drug.

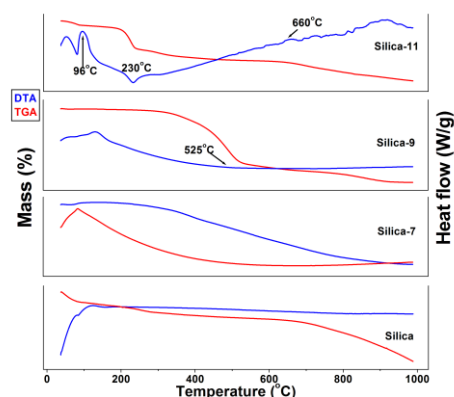


Fig. (3): Thermal behaviour of the drug-free and drug- load silica nanoparticles.

3.4 Morphological, size and surface charge analyses of drug loaded silica

The morphology, size and surface charge of the designed drug-free silica nanoparticles were investigated by TEM and confirmed by zeta-sizer. Figure (4) demonstrated the TEM images of the drug-free silica nanoparticles versus the drug-free loaded silica nanoparticles. The mono-dispersity and the porous microstructure are obviously noted for the drug-free silica nanoparticles (Figure 4a). In addition, the measured diameter of the silica nanoparticles by using TEM was in the range of $40\text{--}50\text{nm}$. In case of drug-loaded silica nanoparticles with compounds, **7** or **11**, the maximum inclusion within the pores of the silica nanoparticles was manifested (Figure 4b and 4d) respectively. Contradictory, compound **9** was not completely encapsulated within the pores of the silica nanoparticles (Figure 4c); most of the drug particles were adsorbed on the surface of the silica nanoparticles. This was confirmed by the increased particle size determined by zeta-sizer curves demonstrated in Figure (5).

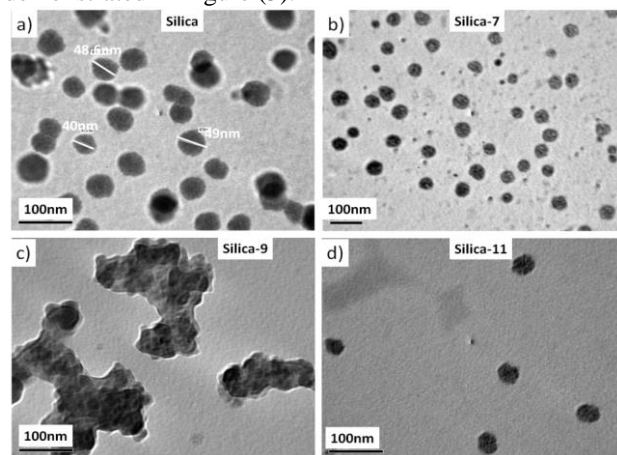


Fig. (4). TEM images for the drug-free silica nanoparticles compared to the drug-loaded silica nanoparticles.

In details, the drug-free silica nanoparticles showed very narrow peak between 17-75nm with maximum intensity at 21.75 nm (Figure 5). This peak was shifted to the range of 200-500 nm with maximum intensity at 292 nm for compound 7-loaded silica nanoparticles. Also, the silica nanoparticles loaded with compound 11 revealed peak in the range of 250-300 nm with maximum intensity at 271nm. Moreover, for the compound 11-loaded silica nanoparticles, additional peak was

detected in the range of 700-1300nm with maximum intensity at 973nm. Of note, the sizes of the drug-free silica as well as the drug-loaded silica nanoparticles measured by zeta-sizer are consistent with those measured by TEM images. The effect of the loaded drugs on the surface charge of the silica nanoparticles were assessed using zeta potential measured by the zeta-sizer instrument as illustrated in Figure (6).

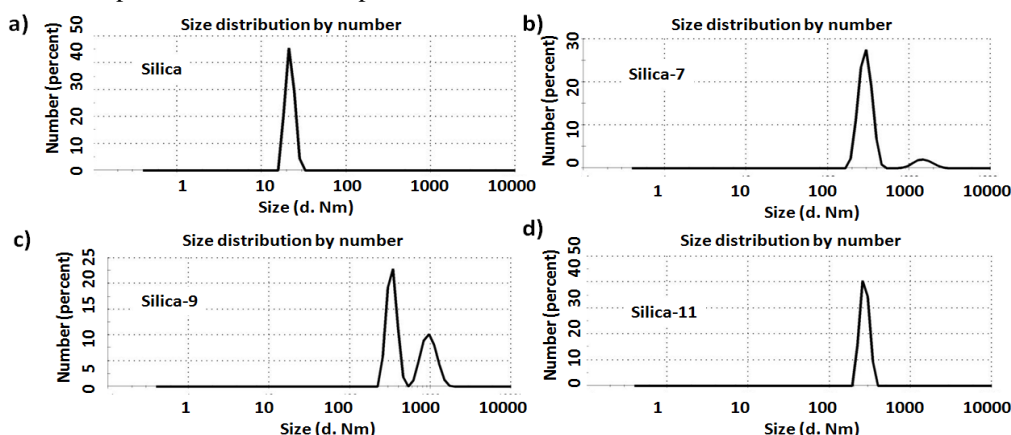


Fig. (5): The particle size of the drug-loaded silica nanoparticles with reference to drug-free silica nanoparticles determined by zeta-sizer.

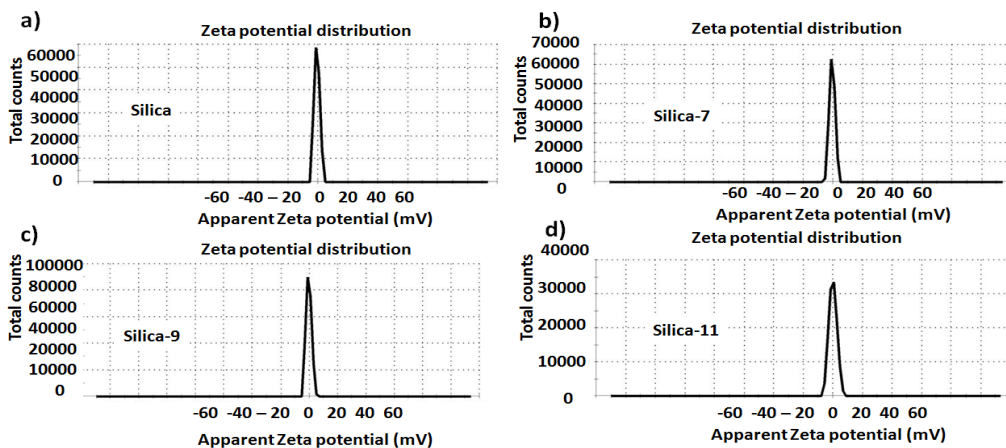


Fig. (6): Zeta potential of the drug-loaded silica nanoparticles with reference to pure silica nanoparticles determined by zeta-sizer.

The data in Fig (6) revealed that all the prepared samples have no changes on the surface charge before and after drug loading. The parameters related to the microstructure of the silica nanoparticles, including surface area, mean pore volume and mean pore diameter were estimated using BET surface area measurements as listed in Table (2). From this table it is obvious that the higher surface area and mean pore volume were attributed to the drug-free silica nanoparticles (160.443 m²/g, pore diameters, from 12-15 nm and 0.7770 cm³/g respectively) compared to the drug-

loaded silica nanoparticles (table 2). For pore diameter of sample silica-7 it is slightly extended from 18-22 nm with mean pore volume = 0.2874cm³/g and surface area of approximately 23.849 m²/g which relatively smaller surface area when compared with silica. The pore size distribution of sample silica-9 that was relatively larger with range of 18-22nm as compared with the S0, mean pore volume = 0.3900 cm³/g and surface area of about 28.369 m²/g. Silica-11 possess surface area approximately 61.026 m²/g which considered higher surface area when compared with the other

two samples (silica-7 and silica-9). Contradictory, relative increase in the mean pore diameter in case of drug -loaded silica nanoparticles was attributed to the loading of the drug within silica nanoparticles (table 2).

3.5 In vitro drug release

The drug release behavior of drug-loaded silica was evaluated in vitro in PBS as illustrated in Figure (7). It was found that the lowest drug release rate was exhibited by silica nanoparticles-loaded with compound-9, where 22.22% of compound 9 was released after the whole immersion time (672 hours). The medium release rate was demonstrated by silica

Table (2): Parameters evaluated by the BET surface area measurements

| Samples | BET Surface area (m ² /g) | Mean Pore volume (cm ³ /g) | Mean Pore diameter (nm) |
|-----------|--------------------------------------|---------------------------------------|-------------------------|
| Silica | 160.443 | 0.7770 | 12-15 |
| Silica-7 | 23.849 | 0.2874 | 18-22 |
| Silica-9 | 28.369 | 0.3900 | 18-22 |
| Silica-11 | 61.026 | 0.7048 | 18-22 |

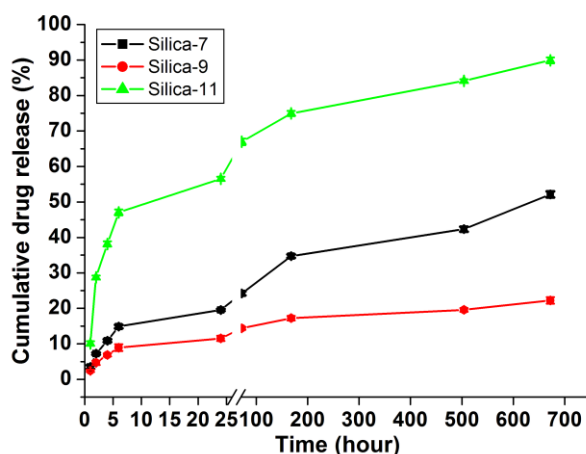


Fig. (7): Release behavior of drug-loaded silica nanoparticles in PBS up to 672 hours.

3.6. In vivo findings

3.6.1. Anthropometric measurements

The results of the current study demonstrated a significant increase ($P < 0.05$) in the body weight, thoracic circumference (TC), abdominal circumference (AC) and body mass index (BMI) of the Mets group with respect to the control group. On the opposite side, significant decrease ($P < 0.05$) in the body weight and TC is detected in Mets groups treated with SMc, **S7**, **S9**, **S11**, **7**, **9** or **11** relative to the Mets group. There is significant reduction ($P < 0.05$) in the AC of Mets group treated with **9** versus Mets group (Table 3). But, there is an insignificant drop ($P > 0.05$) in AC of Mets groups

nanoparticles loaded with compound -7, where 52.13% of compound 7 was released after the whole immersion time (672 hours). The highest release rate was demonstrated by silica nanoparticles loaded with compound-11, where 89.91% of compound 11 was released after the whole immersion time (672 hours) (Fig. 7). This would cause the carried drug molecules to be released at relatively higher rates. Ideally, it is hypothesized that the sustained release of drug could be achieved when the carried drug molecules. Similar results were early reported for the great influence of these parameters on the drug release profiles. (13)

treated with SMc, **S7**, **S9**, **S11**, **7** or **11** compared to the Mets group. Significant decline ($P < 0.05$) in BMI of Mets group treated with SMc, **S7**, **S9**, **S11**, **7** or **11** is observed versus the Mets group. But, insignificant depletion ($P > 0.05$) in BMI of Mets group treated with **9** when compared with Mets group (Table 3).

3.6.2. Biochemical outcomes

The results represented in Table (4) revealed the influence of treatment with SMc, **S7**, **S9**, **S11**, **7**, **9** or **11** on lipid panel (cholesterol, triglycerides, HDL and LDL) of Mets bearing mice. The data revealed that there is a significant rise ($P < 0.05$) in serum cholesterol, triglycerides and LDL levels in the Mets group as compared to the control

group. Meanwhile, the serum HDL level recorded a significant drop ($P < 0.05$) in the Mets group versus the control group. On the opposite hand, treatment of the Mets group with SMC, **S7**, **S9**, **S11**, **7**, **9** or **11** elicited significant reductions ($P < 0.05$) in serum cholesterol, triglycerides and LDL levels when compared with those in the Mets group. Regarding the serum HDL level, treatment of the Mets group with SMC, **S7**, **S11**, **7**, **9** or **11** experienced significant enhancements ($P < 0.05$) in serum HDL level in comparison with that recorded in the Mets group (Table 4). But, treatment of Mets groups with **S9** evoked insignificant raise ($P > 0.05$) in serum HDL level in respect with that in the Mets group.

The results of the current approach revealed a significant increase ($P < 0.05$) in serum glucose, insulin levels, and insulin resistance value in the Mets group versus the control group. Meanwhile, significant decrease ($P < 0.05$) in serum spexin level has been recorded in the Mets group relative to the control group. On the other side, treatment of the Mets group with SMC, **S7**, **S9**, **S11**, **7**, **9** or **11** yielded a significant reduction ($P < 0.05$) in serum glucose level relative to that in the Mets group (Table 5). Treatment of the Mets group with **S11**, **9** or **11** caused a significant decrease ($P < 0.05$) in serum insulin level in comparison with that in the Mets group. But, treatment of the Mets group with SMC, **S7**, **S9** or **7** produced an insignificant drop ($P > 0.05$) in serum insulin level when compared comparison with that in the Mets group. Treatment of Mets group with SMC, **S7**, **S9**, **S11**, **7**, **9** or **11** elicited significant decline ($P < 0.05$) in insulin resistance value versus the Mets group. Treatment of the Mets group with SMC and **S11** provoked significant enhancement ($P < 0.05$) in serum spexin level in comparison with that in the Mets group. But treatment of the Mets group with **S7**, **S9**, **7**, **9** or **11** triggered an insignificant increase ($P > 0.05$) in serum spexin level versus the Mets group.

The obtained data recorded in Table (6) revealed significant elevation ($P < 0.05$) in serum MDA, NO and H_2O_2 levels in the Mets group relative to the control group. However, treatment of Mets group with SMC, **S7**, **S9**, **S11**, **7**, **9** or **11** induced significant reductions ($P < 0.05$) in serum MDA, NO and H_2O_2 levels versus the Mets group.

The present study was initiated to synthesize new heterocyclic steroid derivatives under solvent-free conditions using grinding mortar. Another goal of the study was to load the designed compounds on mesoporous silica nano particles as drug carriers. The study was further extended to explore the efficacy of these entities in antagonizing obesity –associated metabolic syndrome induced in mice.

The physicochemical characterization of the prepared mesoporous silica nanoparticles revealed that they have an amorphous nature that is not changed after drug loading as confirmed by XRD represented in Figure (1). The chemical interaction between the mesoporous silica nanoparticles and the loaded drugs is proved by FTIR as indicated in Figure (2). Moreover, the drug loading within the mesoporous silica nanoparticles is documented by the onset of the difference in weight loss and the changes in the thermal behavior compared to drug-free mesoporous silica nanoparticles detected by DTA/TGA findings as illustrated in Figure (3). The porous nature of the mesoporous silica nanoparticles and the effect of the drug loading on the final morphology, surface charges and the microstructure properties, of the mesoporous silica nanoparticles are approved by the means of TEM and zeta-sizer as represented in Figures (4-6). From the abovementioned results, it could be suggested that the drug composition (chemical and physical properties) defined the way by which the drug is loaded into the mesoporous silica nanoparticles. Accordingly, the release behavior of drug-loaded mesoporous silica nanoparticles is also dependent on the drug composition. This hypothesis is highly appreciated from the different morphologies of drug-loaded mesoporous silica nanoparticles as described in Figure (4). Where the dispersed particles are observed for 1,3-oxathiolane derivatives-loaded mesoporous silica nanoparticles (silica-**7** and silica-**11**) as manifested in Figure (4 b,d). Meanwhile, mesoporous silica nanoparticles loaded with 1,3-oxathiolane derivative (silica-**9**) showed agglomerated particles and most of the compound seems to be adsorbed on the surface of mesoporous silica nanoparticles as evidenced in Figure (4c). This explains the different release behavior (low release profile) of 1,3-oxathiolane derivative loaded on mesoporous silica nanoparticles. This finding is confirmed also by non-homogenous particle distribution recorded for the same sample by zeta-sizer as shown in Figure (5c). In spite of the different release rate observed for each compound by using mesoporous silica nanoparticles as drug delivery vehicles, these nanostructured compounds maintain sustained release up to 672 hours. Previous studies highlighted that the sustained drug release from mesoporous silica nanoparticles is a result of a controlled degradation of the mesoporous silica nanoparticles in the PBS [38]. Parameters controlling the degradation include; morphology, chemical composition, surface functionalization, loaded drug and physiological environment, which coordinate in *in vitro* degradation [39]. In addition,

the surface area plays a fundamental role in the degradation rates of mesoporous silica nanoparticles. Thus, the higher the surface area, the faster the silica matrix lixiviation was reported owing to the better contact with the physiological medium [40].

Regarding the biological application of the newly synthesized compounds loaded on mesoporous silica nanoparticles for management of Mets in mice, the present results revealed a significant increase in anthropometric parameters (TC, AC and BMI) in the Mets group versus the control group. These findings are on par with the study done by **Nago Sock et al.** [41] who reported that there is fat accumulation in the thoracic and abdominal regions of rats due to the high fructose diet. The increase of fructose consumption is associated with an increase in total energy intake and/or certain micronutrient deficiency which may cause Mets [42]. This implies that the detected increase in body weight is attributed to exaggerated energy intake and adipose tissue accumulation. BMI has been declared to be a simple, reliable estimate of body fat accumulation as a positive correlation between daily fat intake and BMI as well as fat deposition [43]. In contrast, there was a significant decrease in the anthropometric para

meters (TC, AC and BMI) in Mets groups treated with SMc, **S7**, **S9**, **S11**, **7**, **9** and **11** relative to the Mets group. These findings could be attributed to the sulfur atom in the newly designed compounds. This explanation is greatly supported by the previous studies done on the natural resources of sulfur compounds. The studies on allium species indicated that they contain precursors of sulfur-containing flavor compounds [44] which have been used in folk medicine for of metabolic disease treatment. Also, more recent study demonstrated that allium-derived extracts showed antiobesity response [45]. The antiobesity and hypolipidemic impacts of *Allium hookeri* were examined in obese mice induced by high-fat diet [46]. A significant suppression in body weight gain and fat accumulation in these mice was demonstrated upon treatment with *A. hookeri*. These results were interpreted as the sulfur containing compounds in the allium are responsible for these effects [43]. This leads us to suggest that our newly synthesized compounds with their sulfur atom may behave similarly as the natural sources containing sulfur regarding their effect on the anthropometric measurements.

The data of the current study demonstrated marked dyslipidemia in Mets group versus the control group. The obtained data are in harmony with **Ostos et al.** [47] who found hypercholesterolemia and hypertriglyceridemia in rats fed on the high fructose diet. More in detail, **Mamo et al.** [48] stated that lipids in adipose tissue

are mainly derived from circulating triglycerides particularly during high-fructose diet feeding. The elevated serum LDL level in Mets rats has been also reported in the high fructose diet supplemented rats [49]. This event is interpreted by the reduced HDL level, as observed in our study, which causes a decline in the reverse cholesterol transport from the blood stream to the liver [50]. Additionally, high fructose diet results in oxidative stress resulting in the enhanced output of reactive oxygen species (ROS) [51]. An increasing scientific report provided ample direct and indirect evidences that the overproduction of ROS can cause cellular deterioration *via* oxidation of critical cellular components such as membrane lipids, proteins, and DNA. So, the elevated level of blood cholesterol, especially LDL is considered as a common risk factor for high fructose diet [49].

Oxidation of LDLs is regarded as a contributing factor in Mets. The increase of cholesterol by fructose may be attributed to elevated amounts of advanced glycation end products, which induce damage to LDL and achieve poor recognition of LDL by lipoprotein and scavenger receptors [52]. Moreover, extreme feeding on fructose may destroy the function of adipocytes and suppress the recycling of cholesterol extracted from serum LDL. Also, the enhancement of uric acid due to high fructose intake may contribute to the increased LDL level [53].

The data represented in Table (4) revealed the influence of treatment with SMc, **S7**, **S9**, **S11**, **7**, **9** or **11** on lipid panel (cholesterol, triglycerides, HDL and LDL) of Mets bearing mice. Treatment of the Mets group with SMc, **S7**, **S9**, **S11**, **7**, **9** or **11** brought about a significant drop in serum cholesterol, triglycerides and LDL levels when compared with those in the Mets group. Regarding the serum HDL level, the treatment of the Mets group with SMc, **S7**, **S11**, **7**, **9** or **11** experienced significant enhancements in serum HDL level in comparison with that recorded in the Mets group. But, treatment of Mets groups with **S9** evoked insignificant rise in the serum HDL level when compared with that in the Mets group. The natural origin of sulfur is a compound called allicin, a common compound in allium species, which showed a favourable effect in reducing blood cholesterol, triglycerides, and glucose levels. Allicin belongs to thiosulfinate compounds, displayed a beneficial effect on the lipid profile in ICR mice causing a distinct decrease in the serum TC, LDL-C [54]. The hypocholesterolemic action of organosulfur compounds has been shown to be due to the inhibition of lipogenic and cholesterogenic enzymes [55]. In addition, it has been found that Thiol compounds have been shown to inhibit oxidation of LDL cholesterol (LDLs) [56].

The present results recorded significant increase in serum glucose, insulin levels and insulin resistance value in the Mets group when compared with the control group. This finding is in keeping with the previous finding of [21]. High Consumption of fructose is believed to be a widespread risk factor in the development of hyperglycemia and whole body insulin resistance [57]. An increased glucose level is a generic feature of obesity itself and its associated metabolic diseases [19]. In this concern, high fructose diet-induced obesity is directly linked with an increased risk of type 2 diabetes [21]. Obesity is a disorder of energy imbalance and is corrected with hyperinsulinemia, insulin resistance and abnormalities in lipid metabolism [58]. The existence of high lipolytic

activity in the accumulated fat leads to high free fatty acids mobilization to the liver. The enhanced fatty acids flux to liver promotes gluconeogenesis and reduces the impact of insulin on peripheral glucose disposal [59]. Also, it has been recorded that obesity is accompanied by low-grade chronic systemic inflammation, which likely results in insulin resistance [60]. The increased morbidity associated- obesity is supposed to be mediated mostly by insulin resistance, diabetes, hypertension, and lipid disorders events [61]. Insulin signaling in adipose tissue plays an essential role in lipid storage and regulation of glucose homeostasis. Thus, insulin signaling in adipocytes is crucial for development of obesity and its associated metabolic abnormalities [62].

Table (3): Effect of treatment with drug-free mesoporous silica nanoparticles, drug-loaded mesoporous silica nanoparticles and free drugs on the anthropometric measurements of Mets bearing mice.

| Parameters | Body weight (g) | Thoracic (cm) | Abdominal (cm) | BMI (g/cm ²) |
|----------------------|------------------------|------------------------|-------------------------|--------------------------|
| Control group | 27.1±0.6 | 9.1±0.34 | 9.2±0.27 | 0.25±0.008 |
| Mets group | 42.5±0.68 ^a | 10.5±0.23 ^a | 10.05±0.15 ^a | 0.37±0.016 ^a |
| Mets + SMc | 35.7±1.1 ^b | 9.3±0.24 ^b | 9.7±0.23 | 0.3±0.01 ^b |
| Mets +S7 | 35.4±1.69 ^b | 9.1±0.3 ^b | 9.6±0.37 | 0.305±0.009 ^b |
| Mets +S9 | 34.7±1.26 ^b | 8.7±0.23 ^b | 9.9±0.2 | 0.32±0.011 ^b |
| Mets +S11 | 34.9±1.16 ^b | 8.8±0.25 ^{bc} | 9.7±0.13 | 0.31±0.009 ^b |
| Mets +7 | 36.0±1.5 ^b | 9.2±0.26 ^b | 9.8±0.08 | 0.32±0.009 ^b |
| Mets +9 | 35.4±0.45 ^b | 8.6±0.15 ^b | 9.4±0.2 ^b | 0.34±0.005 |
| Mets +11 | 36.1±0.74 ^b | 9.74±0.22 ^b | 9.8±0.17 | 0.3±0.015 ^b |

Data are represented as Mean ± S.E of 10mice/group.

a: Significant change at P<0.05 in comparison with the control group. b: Significant change at P<0.05 in comparison with the Mets group. c: Significant change at P<0.05 in comparison between free drug groups in respect with the corresponding mesoporous silica-loaded drug nanoparticles groups.

Table (4): Effect of treatment with drug-free mesoporous silica nanoparticles, drug-loaded mesoporous silica nanoparticles and free drugs on lipid panel of Mets bearing mice.

| Parameters | Cholesterol (mg/dL) | Triglycerides (mg/dL) | HDL (mg/dL) | LDL (mg/dL) |
|----------------------|-------------------------|---------------------------|------------------------|-------------------------|
| Control group | 66.7±2.76 | 71.28±3.03 | 34.6±0.92 | 20.6±3.82 |
| Mets group | 141.9±4.2 ^a | 117.15±8.43 ^a | 23.5±0.49 ^a | 99.6±4.97 ^a |
| Mets + SMc | 87.2±2.17 ^b | 95.09±2.35 ^b | 32.8±1.7 ^b | 39.2±2.17 ^b |
| Mets +S7 | 82.4±1.31 ^{bc} | 90.36±3.23 ^b | 33.6±1.1 ^b | 34.3±1.59 ^{bc} |
| Mets +S9 | 87.9±1.7 ^b | 89.78±3.35 ^b | 26.7±1.9 ^c | 46.8±3.19 ^b |
| Mets +S11 | 88.3±3.39 ^b | 116.07±4.18 ^{bc} | 27.7±0.8 ^{bc} | 42.0±3.62 ^b |
| Mets +7 | 99.1±4.58 ^b | 92.52±2.9 ^b | 32.05±2.3 ^b | 52.3±5.35 ^b |
| Mets +9 | 87.04±5.69 ^b | 91.19±3.61 ^b | 33.3±0.95 ^b | 39.1±6.22 ^b |
| Mets +11 | 94.8±5.821 ^b | 95.28±3.5 ^b | 32.6±1.99 ^b | 46.9±6.06 ^b |

Data are represented as Mean ± S.E of 10 mice/group.

a: Significant change at P<0.05 in comparison with the control group.

b: Significant change at P<0.05 in comparison with the obese group.

c: Significant change at P<0.05 in comparison between free drug groups in respect with corresponding mesoporous silica-loaded drug nanoparticles groups.

Table (5): Effect of treatment with drug-free mesoporous silica nanoparticles, drug-loaded mesoporous silica nanoparticles and free drugs on serum glucose, insulin, spexin and insulin resistance and spexin values of Mets bearing mice.

| Parameters Groups | Glucose (mg/dL) | Insulin (μ U/ml) | insulin resistance value | Spexin (ng/L) |
|----------------------|-------------------------------|------------------------------|------------------------------|--------------------------------|
| Control group | 63.7 \pm 2.9 | 12.8 \pm 0.45 | 2.01 \pm 0.12 | 263.1 \pm 8.36 |
| Mets group | 133.0 \pm 8.18 ^a | 21.3 \pm 0.62 ^a | 7.04 \pm 0.53 ^a | 150.9 \pm 5.43 ^a |
| Mets + SMc | 83.6 \pm 6.69 ^b | 17.7 \pm 0.98 | 3.6 \pm 0.32 ^b | 180.3 \pm 6.27 ^b |
| Mets +S7 | 73.5 \pm 4.7 ^b | 17.4 \pm 2.38 | 3.2 \pm 0.48 ^b | 163.2 \pm 2.14 |
| Mets +S9 | 74.6 \pm 8.48 ^b | 17.8 \pm 2.7 | 3.03 \pm 0.4 ^b | 166.9 \pm 7.21 |
| Mets +S11 | 97.7 \pm 5.4 ^{bc} | 16.2 \pm 0.99 ^b | 3.8 \pm 0.2 ^b | 202.8 \pm 5.24 ^{bc} |
| Mets +7 | 80.8 \pm 4.6 ^b | 17.5 \pm 1.15 | 3.4 \pm 0.27 ^b | 154.6 \pm 4.57 |
| Mets +9 | 80.9 \pm 4.3 ^b | 17.2 \pm 1.05 ^b | 3.39 \pm 0.23 ^b | 151.3 \pm 7.79 |
| Mets +11 | 75.4 \pm 5.2 ^b | 16.3 \pm 1.13 ^b | 3.06 \pm 0.3 ^b | 152.5 \pm 7.83 |

Data are represented as Mean \pm S.E of 10 mice/group.

a: Significant change at P<0.05 in comparison with the control group.

b: Significant change at P<0.05 in comparison with the Mets group.

c: Significant change at P<0.05 in comparison between free drug group in respect with corresponding mesoporous silica-loaded nanoparticles groups.

Table (6): Effect of treatment with drug-free mesoporous silica nanoparticles, drug-loaded mesoporous silica nanoparticles and free drugs on oxidative stress status of Mets bearing mice.

| Parameters Groups | MDA (nmol/mL) | NO (μ mol/L) | H ₂ O ₂ (mM/L) |
|----------------------|-------------------------------|--------------------------------|---|
| Control group | 40.5 \pm 1.06 | 63.1 \pm 2.42 | 0.108 \pm 0.011 |
| Mets group | 81.8 \pm 1.62 ^a | 129.6 \pm 6.66 ^a | 0.42 \pm 0.033 ^a |
| Mets + SMc | 47.1 \pm 0.92 ^b | 97.1 \pm 4.65 ^b | 0.28 \pm 0.018 ^b |
| Mets +S7 | 54.5 \pm 1.66 ^b | 102.5 \pm 6.18 ^{bc} | 0.17 \pm 0.011 ^b |
| Mets +S9 | 55.8 \pm 2.23 ^{bc} | 73.7 \pm 5.8 ^b | 0.16 \pm 0.011 ^{bc} |
| Mets +S11 | 60.9 \pm 3.51 ^b | 107.3 \pm 9.45 ^b | 0.22 \pm 0.026 ^b |
| Mets +7 | 56.6 \pm 4.31 ^b | 106.5 \pm 5.52 ^b | 0.28 \pm 0.024 ^b |
| Mets +9 | 46.4 \pm 2.98 ^b | 109.5 \pm 7.04 ^b | 0.14 \pm 0.008 ^b |
| Mets +11 | 60.6 \pm 2.92 ^b | 102.02 \pm 7.7 ^b | 0.22 \pm 0.026 ^b |

Data are represented as Mean \pm S.E of 10 mice/group.

a: Significant change at P<0.05 in comparison with the control group.

b: Significant change at P<0.05 in comparison with the Mets group.

c: Significant change at P<0.05 in comparison between free drug groups in respect with the corresponding mesoporous silica-loaded drug nanoparticles groups

In the present approach, the elevated level of blood glucose induced by high fructose diet was ameliorated by the newly synthesized compounds. Besides, these compounds prevented hyperinsulinemia and insulin resistance. The present results go hand in hand with those of Yang et al. [63] who stated that sulfur containing compounds contributes to lowering the elevated blood glucose level and improving insulin sensitivity in obesity. In addition, testosterone plays a role in the treatment of the metabolic syndrome and its sequels such as diabetes mellitus type 2 and cardiovascular disease [64]. Moreover, it has been reported [65] that some steroid derivatives induce changes of glucose levels and thus steroid derivatives could be responsible for the reducing serum glucose level in the current study. The steroid derivatives exert this effect

depending on its physicochemical properties which could be related to the degree of lipophilicity of the steroid derivative [66]. Furthermore, testosterone has been found to reduce insulin levels and insulin resistance in men with obesity [67]. Additionally, administration of Allium apparently prohibited the body weight gain and amended insulin resistance in C57BL/6J obese mice [63].

Spexin (SPX) is a novel peptide hormone initially recognized using a computational method based on Markov model screening to identify novel biologically active peptides [68]. The serum SPX levels were detected to be low in T2DM patients and inversely related to blood glucose and lipids, indicating its possible role in glucose and lipid metabolism [69]. Decreased serum levels of the SPX are modestly accompanied by components of

metabolic syndrome [70]. The present data registered a significant drop in serum SPX level in Mets mice as compared to the control counterparts. It has been reported that patients having more than one metabolic syndrome component at the same time exhibited a significant decrease in SPX levels compared to those having less risk factors. Furthermore, the study of **Lin et al.** [71] proved that serum SPX levels are significantly negatively correlated with BMI, fasting glucose and triglycerides and SPX levels independently predict the risk of high BMI and high fasting glucose. **Sassek et al.** [72] concluded that SPX may be highly implicated in the pathogenesis of diabetes or its recovery due to the effect of SPX on insulin secretion *in vitro* and *in vivo*. Moreover, **Lin et al.** [73] emphasized the role of the SPX in bile acid synthesis and proved a correlation between serum SPX and total cholesterol in rats. However, the precise mode of action of the SPX is still uncertain because of the lack of data on the SPX receptor [74]. Meanwhile, Evidences are accumulating, and suggesting multiple physiological functions of SPX because of its expression in various tissues.

In this study the newly synthesized compounds exerted significant elevation in the serum SpX level in Mets mice when compared with the Met bearing mice. This may be related to the modulation of BMI, dyslipidemia, as well as glucose level upon treatment with these compounds. As, there is an inverse correlation between the serum SPX level and the Mets components [70] Also, **Lin and his co-workers** emphasized this hypothesis as they found that serum SPX levels are significantly negatively correlated with BMI, fasting glucose, cholesterol and triglycerides [71].

The present findings demonstrated significant elevation serum MDA, NO and H₂O₂ in the Mets group relative to the control group. The study of **Vincent and Taylor** [75] concluded the significant relationship between obesity and prooxidants which showed great support to our results. Obesity-associated Mets promotes inflammation, which in turn induces an increase in free radicals and subsequently triggering oxidative stress [76]. It has also been reported that obesity *per se* can promote systemic oxidative stress: indeed, fat accumulation increases Nox activity and endoplasmic reticulum (ER) stress in adipocytes that result in increased ROS production [77, 78]. Increased levels of these extremely reactive species can deteriorate DNA, lipids, and proteins [79]. Obese patients exhibit higher oxLDL, AAOPs and TBARs levels than control counterparts [80]; these biomarkers can anticipate the development and progression of metabolic and CVD in overweight and obese

subjects [81, 82]. The reduction in body fat in obese subjects decreases oxidant production and, in turn, the onset of obesity related diseases [83].

Treatment with the newly synthesized compounds in the present work exhibited a significant drop in serum oxidative stress markers (MDA, NO and H₂O₂) in Mets mice as compared to the Mets bearing mice. The effect of the newly synthesized compounds on oxidative stress markers indicates their efficacy in scavenging free radicals. It has been demonstrated that sulfur compounds possess a potent role in redox reactions as thiol compounds have antioxidant actions [56]. Also, it has been mentioned that compounds containing sulfhydryl groups have great potency for scavenging free radicals [84]. In addition, it has been documented that the steroidal heterocyclic compounds possess a significant antioxidant activity [85]. The *in vitro* antioxidant activity and scavenging free radicals effect of heterocyclic steroidal compounds were evaluated by using different reactive species assays containing DPPH radical. The antioxidant effect and scavenging free radicals ability of the heterocyclic steroidal compounds could be due to their hydrogen donating ability [86, 87]. More recent study demonstrated that the antioxidant activity of the heterocyclic steroids has been attributed to: (1) binding of transition metal ion catalysts, (2) decomposition of peroxides, (3) prevention of continuous proton abstraction and (4) radical scavenging activity [88].

Collectively, previous studies asserted that when heterogeneous ring compounds containing nitrogen, oxygen and sulfur atoms are added to steroid compounds skeleton A- and D rings [89], at their biological activity such as being hypotensive, hypocholesterolemic and diuretic activities are enhanced [90]. This may explain the superior activity **S11** as it was modified by adding rings containing sulfur atoms to its skeleton at the A- and D rings beside loading on MSNs. Compound **7** came after **S11** due to adding hetero ring containing a sulfur atom on A ring only. However, the activity of **S9** could be attributed to modification of steroid moiety at D ring only beside loading on MSNs. Meanwhile, compound **9** showed less activity than the compound **S9** as it wasn't loaded on MSNs.

4. Conclusion

The results of the present investigation indicate the effectiveness of drug loaded on mesoporous silica nanoparticles in mitigation of metabolic syndrome induced by high fructose diet. The present data provide an experimental evidence for the preferable therapeutic action of 1,3-oxathiolane steroid

derivatives as novel molecules against metabolic syndrome components. This was documented by antihyperlipidemic, hypoglycemic, and antihyperinsulinemic response in addition to the free radical scavenging activity of these compounds. Noteworthy, **S11** compound exerts the superior effect due to modification of the steroid moiety at A and D rings in addition to its loading on mesoporous silica nanoparticles.

5. Conflicts of interest

There are no conflicts to declare.

6. Funding

This work was financially supported by National Research Centre, Cairo, Egypt (NRC).

7. References

1. Gao, M. and D. Liu, *Controlling obesity and metabolic diseases by hydrodynamic delivery of a fusion gene of Exendin-4 and $\alpha 1$ Antitrypsin*. Scientific reports, 2019. **9**(1): p. 1-12.
2. Yu, S., et al., *An update on the prevalence of metabolic syndrome and its associated factors in rural northeast China*. BMC Public Health, 2014. **14**(1): p. 1-9.
3. Murdolo, G., et al., *Oxidative stress and lipid peroxidation by-products at the crossroad between adipose organ dysregulation and obesity-linked insulin resistance*. Biochimie, 2013. **95**(3): p. 585-594.
4. Grundy, S.M., *Drug therapy of the metabolic syndrome: minimizing the emerging crisis in polypharmacy*. Nature reviews Drug discovery, 2006. **5**(4): p. 295-309.
5. Ioannides-Demos, L.L., L. Piccenna, and J.J. McNeil, *Pharmacotherapies for obesity: past, current, and future therapies*. Journal of obesity, 2011. **2011**.
6. Kang, J.G. and C.-Y. Park, *Anti-obesity drugs: a review about their effects and safety*. Diabetes & metabolism journal, 2012. **36**(1): p. 13-25.
7. Sharkey, L.C., et al., *Effect of ovariectomy and estrogen replacement on cardiovascular disease in heart failure-prone SHHF/Mcc-fa cp rats*. Journal of molecular and cellular cardiology, 1999. **31**(8): p. 1527-1537.
8. Anderson, J.W. and E.C. Konz, *Obesity and disease management: effects of weight loss on comorbid conditions*. Obesity research, 2001. **9**(S11): p. 326S-334S.
9. Kapoor, D., et al., *Testosterone replacement therapy improves insulin resistance, glycaemic control, visceral adiposity and hypercholesterolaemia in hypogonadal men with type 2 diabetes*. European Journal of Endocrinology, 2006. **154**(6): p. 899-906.
10. Salvador, J.A., et al., *Anticancer steroids: linking natural and semi-synthetic compounds*. Natural product reports, 2013. **30**(2): p. 324-374.
11. Müller-Schiffmann, A., H. Sticht, and C. Korth, *Hybrid compounds*. BioDrugs, 2012. **26**(1): p. 21-31.
12. Vallet-Regí, M., F. Balas, and D. Arcos, *Mesoporous materials for drug delivery*. Angewandte Chemie International Edition, 2007. **46**(40): p. 7548-7558.
13. Watermann, A. and J. Brieger, *Mesoporous silica nanoparticles as drug delivery vehicles in cancer*. Nanomaterials, 2017. **7**(7): p. 189.
14. Esmaeili, A. and S.N. Mousavi, *Synthesis of a novel structure for the oral delivery of insulin and the study of its effect on diabetic rats*. Life sciences, 2017. **186**: p. 43-49.
15. Zhao, S., et al., *One-step synthesis of core-shell structured mesoporous silica spheres templated by protic ionic liquid and CTAB*. Materials Letters, 2016. **178**: p. 35-38.
16. Fuente, A., et al., *$1H$ and $13C$ NMR spectral assignment of androstane derivatives*. Magnetic Resonance in Chemistry, 2005. **43**(8): p. 676-678.
17. Tigineh, G.T., Y.-S. Wen, and L.-K. Liu, *Solvent-free mechanochemical conversion of 3-ethoxysalicylaldehyde and primary aromatic amines to corresponding Schiff-bases*. Tetrahedron, 2015. **71**(1): p. 170-175.
18. Paul, A., T. Warner, and C. John, *Green chemistry: theory and practice*. Oxford [England], New York: Oxford University Press, 1998. **11**: p. 1394013941.
19. Buettner, R., et al., *Defining high-fat-diet rat models: metabolic and molecular effects of different fat types*. Journal of molecular endocrinology, 2006. **36**(3): p. 485-501.
20. Bagul, P., H. Middela, and S. Matapally, *Padiya r, Bastia T, Madhusudana K, reddy Br, chakravarty S and Banerjee SK: attenuation of insulin resistance, metabolic syndrome and hepatic oxidative stress by resveratrol in fructose-fed rats*. Pharmacol res, 2012. **66**: p. 260-268.
21. Jiang, C., et al., *Dibenzazepine-loaded nanoparticles induce local browning of white adipose tissue to counteract obesity*. Molecular Therapy, 2017. **25**(7): p. 1718-1729.
22. Novelli, E., et al., *Anthropometrical parameters and markers of obesity in rats*. Laboratory animals, 2007. **41**(1): p. 111-119.
23. Meitattini, F., et al., *The 4-hydroxybenzoate/4-aminophenazone chromogenic system used in the enzymic determination of serum cholesterol*. Clinical Chemistry, 1978. **24**(12): p. 2161-2165.

24. Bucolo, G. and H. David, *Quantitative determination of serum triglycerides by the use of enzymes*. Clinical chemistry, 1973. **19**(5): p. 476-482.
25. Naito, H. and A. Kaplan, *High-density lipoprotein (HDL) cholesterol*. Clin. Chem. Toronto. Princeton, 1984: p. 1207-1213.
26. Young, D.S., *Effects of Disease on Clinical Laboratory Tests: Listing by disease*. Vol. 2. 2001: AACC press.
27. Rudovich, N.N., H.J. Rochlitz, and A.F. Pfeiffer, *Reduced hepatic insulin extraction in response to gastric inhibitory polypeptide compensates for reduced insulin secretion in normal-weight and normal glucose tolerant first-degree relatives of type 2 diabetic patients*. Diabetes, 2004. **53**(9): p. 2359-2365.
28. Duncan, M., et al., *A simple measure of insulin resistance*. Lancet (London, England), 1995. **346**(8967): p. 120-121.
29. Aebi, H., *Catalase in vitro Methods Enzymol 105: 121-126*. Find this article online, 1984.
30. Okaichi, Y., et al., *Arachidonic acid improves aged rats' spatial cognition*. Physiology & behavior, 2005. **84**(4): p. 617-623.
31. Dymock, H.M.J., *The determination of nitrite in water*. Analyst 86, 1961. **414**: p. 416.
32. Armitage, P., G. Berry, and J. Matthews, *Comparison of several groups*. Statistical methods in medical research, 1987. **186**: p. 213.
33. Stojanović, D.B., et al., *Transparent PMMA/silica nanocomposites containing silica nanoparticles coating under supercritical conditions*. Progress in Organic Coatings, 2013. **76**(4): p. 626-631.
34. Lungare, S., K. Hallam, and R.K. Badhan, *Phytochemical-loaded mesoporous silica nanoparticles for nose-to-brain olfactory drug delivery*. International journal of pharmaceutics, 2016. **513**(1-2): p. 280-293.
35. Khan, M.A., et al., *Product development studies on sonocrystallized curcumin for the treatment of gastric cancer*. Pharmaceutics, 2015. **7**(2): p. 43-63.
36. Feng, R., Z. Song, and G. Zhai, *Preparation and in vivo pharmacokinetics of curcumin-loaded PCL-PEG-PCL triblock copolymeric nanoparticles*. International journal of nanomedicine, 2012. **7**: p. 4089.
37. Jambhrunkar, S., et al., *Mesoporous silica nanoparticles enhance the cytotoxicity of curcumin*. Rsc Advances, 2014. **4**(2): p. 709-712.
38. Braun, K., et al., *Dissolution kinetics of mesoporous silica nanoparticles in different simulated body fluids*. Journal of Sol-Gel Science and Technology, 2016. **79**(2): p. 319-327.
39. Yu, T., A. Malugin, and H. Ghandehari, *Impact of silica nanoparticle design on cellular toxicity and hemolytic activity*, ACS Nano 5 (2011) 5717-5728. 2012.
40. Huang, X., N.P. Young, and H.E. Townley, *Characterization and comparison of mesoporous silica particles for optimized drug delivery*. Nanomaterials and Nanotechnology, 2014. **4**(Godište 2014): p. 4-2.
41. Sock, E.T.N., et al., *Effects of a short-term overfeeding with fructose or glucose in healthy young males*. British journal of nutrition, 2010. **103**(7): p. 939-943.
42. Lupton, J.R., et al., *Dietary reference intakes for energy, carbohydrate, fiber, fat, fatty acids, cholesterol, protein, and amino acids*. National Academy Press: Washington, DC, USA, 2002. **5**: p. 589-768.
43. Mikaili, P., et al., *Therapeutic uses and pharmacological properties of garlic, shallot, and their biologically active compounds*. Iranian journal of basic medical sciences, 2013. **16**(10): p. 1031.
44. Schutte, L. and R. Teranishi, *Precursors of sulfur-containing flavor compounds*. Critical Reviews in Food Science & Nutrition, 1974. **4**(4): p. 457-505.
45. Joo, H., et al., *Anti-obesity effects of hot water extract and high hydrostatic pressure extract of garlic in rats fed a high-fat diet*. Food and Chemical Toxicology, 2013. **55**: p. 100-105.
46. Buettner, R., Imerich JS, Bollheimer LC. *High-fat diets: modeling the metabolic disorders of human obesity in rodents*. Obesity, 2007. **15**(4): p. 798-808.
47. Ostos, M.A., et al., *Fructose intake increases hyperlipidemia and modifies apolipoprotein expression in apolipoprotein AI-CIII-AIV transgenic mice*. The Journal of nutrition, 2002. **132**(5): p. 918-923.
48. Mamo, J.C., et al., *Partial characterization of the fructose-induced defect in very-low-density lipoprotein triglyceride metabolism*. Metabolism, 1991. **40**(9): p. 888-893.
49. Zhang, Y.H., et al., *Very high fructose intake increases serum LDL-cholesterol and total cholesterol: a meta-analysis of controlled feeding trials*. The Journal of nutrition, 2013. **143**(9): p. 1391-1398.
50. Raveh, O., et al., *Kinetics of lipid peroxidation in mixtures of HDL and LDL, mutual effects*. Free Radical Biology and Medicine, 2001. **31**(11): p. 1486-1497.

51. Delbosc, S., et al., *Involvement of oxidative stress and NADPH oxidase activation in the development of cardiovascular complications in a model of insulin resistance, the fructose-fed rat*. *Atherosclerosis*, 2005. **179**(1): p. 43-49.
52. Zimmermann, R., Panzenbock U, Wintersperger A, Levak-Frank S, Graier W, Glatter O, Fritz G, Kostner GM, and Zechner R. Lipoprotein lipase mediates the uptake of glycated LDL in fibroblasts, endothelial cells, and macrophages. *Diabetes*, 2001. **50**: p. 1643-1653.
53. Perez-Pozo, S.E., et al., *Excessive fructose intake induces the features of metabolic syndrome in healthy adult men: role of uric acid in the hypertensive response*. *International journal of obesity*, 2010. **34**(3): p. 454-461.
54. Lu, Y., et al., *Cholesterol-lowering effect of allicin on hypercholesterolemic ICR mice*. *Oxidative medicine and cellular longevity*, 2012. **2012**.
55. Qureshi, A.A., et al., *Inhibition of cholesterol and fatty acid biosynthesis in liver enzymes and chicken hepatocytes by polar fractions of garlic*. *Lipids*, 1983. **18**(5): p. 343-348.
56. Lynch, J.W., et al., *Income inequality and mortality: importance to health of individual income, psychosocial environment, or material conditions*. *Bmj*, 2000. **320**(7243): p. 1200-1204.
57. Elliott, S.S., et al., *Fructose, weight gain, and the insulin resistance syndrome*. *The American journal of clinical nutrition*, 2002. **76**(5): p. 911-922.
58. Shalaby, H.M.A., et al., *The assessment of some biochemical and immunological effects by amphetamine and orlistat on obesity in rats*. *Food and Public Health*, 2014. **4**(4): p. 185-192.
59. Ginsberg, H.N. and A.F. Stalenhoef, *The metabolic syndrome: targeting dyslipidaemia to reduce coronary risk*. *European Journal of Cardiovascular Prevention & Rehabilitation*, 2003. **10**(2): p. 121-128.
60. Mori, N., et al., *Insulin treatment-induced daily changes to plasma adiponectin and TNF- α level and lipid metabolism parameters in dogs suffering from Type I Diabetes Mellitus*. *Asian Journal of Animal and Veterinary Advances*, 2011. **6**(8): p. 844-850.
61. Zacharie, S., et al., *Body Mass Index as a Risk Factor for Prostate Cancer and Benign Prostate Hypertrophy: a Comparative Study at Three Reference Hospitals in Cameroon*. 2018.
62. Blüher, M., et al., *Adipose tissue selective insulin receptor knockout protects against obesity and obesity-related glucose intolerance*. *Developmental cell*, 2002. **3**(1): p. 25-38.
63. Yang, M.H., et al., *Comparative evaluation of sulfur compounds contents and antiobesity properties of Allium hookeri prepared by different drying methods*. *Evidence-Based Complementary and Alternative Medicine*, 2017. **2017**.
64. Saad, F. and L.J. Gooren, *The role of testosterone in the etiology and treatment of obesity, the metabolic syndrome, and diabetes mellitus type 2*. *Journal of obesity*, 2011. **2011**.
65. Figueroa-Valverde, L., et al., *Activity induced by two Steroid-Dihydropyrimidine derivatives on Glucose levels in a Diabetic Rat Model. Relationship between descriptors logP and π and its Antidiabetic activity*. *International Journal of PharmTech Research*, 2010: p. 2075-2080.
66. Figueroa-Valverde, L., et al., *Antimicrobial activity induced by a steroid-brucine derivative on S. typhi, K. pneumoniae and E. coli*. *Journal of Biological Sciences*, 2014: p. 67-72.
67. Boyanov, M., Z. Boneva, and V. Christov, *Testosterone supplementation in men with type 2 diabetes, visceral obesity and partial androgen deficiency*. *The Aging Male*, 2003. **6**(1): p. 1-7.
68. Mirabeau, O., et al., *Identification of novel peptide hormones in the human proteome by hidden Markov model screening*. *Genome research*, 2007. **17**(3): p. 320-327.
69. Kumar, S., et al., *Decreased circulating levels of spexin in obese children*. *The Journal of Clinical Endocrinology & Metabolism*, 2016. **101**(7): p. 2931-2936.
70. Al-Daghri, N.M., et al., *Spexin levels are associated with metabolic syndrome components*. *Disease markers*, 2018. **2018**.
71. Lin, C.-y., et al., *Circulating spexin levels negatively correlate with age, BMI, fasting glucose, and triglycerides in healthy adult women*. *Journal of the Endocrine Society*, 2018. **2**(5): p. 409-419.
72. Sassek, M., et al., *Spexin modulates functions of rat endocrine pancreatic cells*. *Pancreas*, 2018. **47**(7): p. 904-909.
73. Lin, C.-y., et al., *Spexin acts as novel regulator for bile acid synthesis*. *Frontiers in physiology*, 2018. **9**: p. 378.
74. Kim, D.-K., et al., *Coevolution of the spexin/galanin/kisspeptin family: Spexin activates galanin receptor type II and III*. *Endocrinology*, 2014. **155**(5): p. 1864-1873.
75. Vincent, H.K. and A.G. Taylor, *Biomarkers and potential mechanisms of obesity-induced oxidant stress in humans*. *International journal of obesity*, 2006. **30**(3): p. 400-418.
76. McArdle, M.A., et al., *Mechanisms of obesity-induced inflammation and insulin resistance:*

- insights into the emerging role of nutritional strategies.* *Frontiers in endocrinology*, 2013. **4**: p. 52.
77. Mlinar, B. and J. Marc, *New insights into adipose tissue dysfunction in insulin resistance.* *Clinical Chemistry and Laboratory Medicine (CCLM)*, 2011. **49**(12): p. 1925-1935.
78. Furukawa, S., et al., *Increased oxidative stress in obesity and its impact on metabolic syndrome.* *The Journal of clinical investigation*, 2017. **114**(12): p. 1752-1761.
79. Halliwell, B., *Free radicals and antioxidants: a personal view.* *Nutrition reviews*, 1994. **52**(8): p. 253-265.
80. D'Archivio, M., et al., *Predominant role of obesity/insulin resistance in oxidative stress development.* *European journal of clinical investigation*, 2012. **42**(1): p. 70-78.
81. Krzystek-Korpacka, M., et al., *Advanced oxidation protein products (AOPPs) in juvenile overweight and obesity prior to and following weight reduction.* *Clinical Biochemistry*, 2008. **41**(12): p. 943-949.
82. Codoner-Franch, P., et al., *Elevated advanced oxidation protein products (AOPPs) indicate metabolic risk in severely obese children.* *Nutrition, Metabolism and Cardiovascular Diseases*, 2012. **22**(3): p. 237-243.
83. Virgolici, B., et al., *A comparative oxidative stress study--obesity with and without diabetes mellitus.* *Romanian journal of internal medicine= Revue roumaine de medecine interne*, 2005. **43**(3-4): p. 261-268.
84. Pollack, M. and C. Leeuwenburgh, *Molecular mechanisms of oxidative stress in aging: free radicals, aging, antioxidants and disease.* *Handbook of oxidants and antioxidants in exercise*, 1999. **30**: p. 881-926.
85. Ali, A., et al., *Synthesis and characterization of steroidal heterocyclic compounds, DNA condensation and molecular docking studies and their in vitro anticancer and acetylcholinesterase inhibition activities.* *RSC advances*, 2015. **5**(93): p. 75964-75984.
86. Baumann, J., *Prostaglandin synthetase inhibiting O₂-radical scavenging properties of some flavonoids and related phenolic compounds.* *Naunyn-Schmiedebergs Arch Pharmacol*, 1979. **308**: p. 27-32.
87. Gulcin, I., et al., *Free Rad. Res. Free Rad. Res.* **26**, 469-478, 1997. *Chemical & pharmaceutical bulletin*, 2005. **53**(3): p. 281-285.
88. Baskar, R., et al., *Free radical scavenging activity of antitumour polysaccharide fractions isolated from Ganoderma lucidum (Fr.) P. karst.* 2008.
89. Tantawy, M.A., et al., *Auspicious role of the steroidal heterocyclic derivatives as a platform for anti-cancer drugs.* *Bioorganic chemistry*, 2017. **73**: p. 128-146.
90. Abd Elhalim, M.M., et al., *Synthesis, characterization, and evaluation of cytotoxic effects of novel hybrid steroidal heterocycles as PEG based nanoparticles.* *Asian Pacific journal of cancer prevention: APJCP*, 2017. **18**(7): p. 1937.